Theory of excitonic second-harmonic generation in monolayer MoS$_2$

Mads L. Trolle,[1,][*] Gotthard Seifert,[2] and Thomas G. Pedersen[1,3]

[1]*Department of Physics and Nanotechnology, Aalborg University, Skjernvej 4A, DK-9220, Aalborg East, Denmark*
[2]*Physikalische Chemie, Technische Universität Dresden, D-01062, Dresden, Germany*
[3]*Center for Nanostructured Graphene (CNG), Aalborg University, DK-9220, Aalborg East, Denmark*

Recent experimental results have demonstrated the ability of monolayer MoS$_2$ to efficiently generate second harmonic fields with susceptibilities between 0.1 and 100 nm/V. However, few theoretical calculations exist with which to interpret these findings. In particular, it is of interest to theoretically estimate the modulus of the second harmonic response since experimental reports on this differ by almost three orders of magnitude. Here, we present calculations of the second harmonic response based on a tight-binding band structure and implementation of excitons in a Bethe-Salpeter framework. We compare directly with recent experimental findings demonstrating a good agreement with the excitonic theory regarding, e.g., peak position. Furthermore, we predict an off-resonance susceptibility on the order of 0.1 nm/V, while on-resonance values rise to 4 nm/V.

I. INTRODUCTION

The prediction and observation of a direct band gap in monolayer (ML) MoS$_2$ has revitalized the interest in the optical properties of this material [1–13]. Indeed, the fact that MoS$_2$ is comprised of weakly van der Waals bound layers allows fabrication of samples with atomically well-defined thicknesses by mechanical exfoliation [14]. Following this discovery, a surge of interest in the physical properties of this new two-dimensional material has ensued, revealing promising technological applications in, e.g., field effect transistors [15]. Also, systematic studies of the layer-dependent optical properties of few-layered (FL) MoS$_2$ have been carried out, revealing a remarkable thickness sensitivity in photoluminescence experiments [2,9]. This trend can be attributed to the changing nature of the band gap (going from indirect in the FL and bulk material to direct in ML samples) theoretically predicted already in the work of Mattheiss [16], and more recently, verified using *ab initio* density functional theory (DFT) and quasiparticle GW methods [1,12,17–21]. Monolayer MoS$_2$ is generally reported to display quasiparticle gaps [1,12,21] of ∼2.8 eV, almost 1 eV larger than the corresponding DFT results [1,12,18–21]. Also, optical absorption spectra are very poorly described in the one-electron picture, requiring the inclusion of electron-hole attraction to accurately model photoexcitations, affirming the increased importance of the electron-electron interaction in such two-dimensional systems [1,12,22].

Performing these calculations *ab initio* is typically extremely expensive in terms of the computational resources often resulting in optical spectra based on modest reciprocal space sampling with poor resolution of delicate spectral features, such as discrete excitons or van Hove resonances. Indeed, Qiu *et al.* [12] have recently demonstrated how a convincing agreement between experimental and theoretical absorption spectra can be achieved in the Bethe-Salpeter exciton picture only upon the inclusion of several thousand k points and tens of bands. For other materials, the computational complexity has been reduced by introducing semi-empirical

models based on, for example, the effective-mass Wannier approximation [23]. Another approach is based on models where quasiparticle energies are approximated by, e.g., tight-binding band structures fitted to GW results and where electron-hole attraction is included using an empirical interaction potential, such as the much-used Ohno form [24–27]. This method has proven very successful for both organic [24,25] and inorganic [26] systems. In addition to being of substantial computational advantage, such methods also offer a distilled version of the physics involved, highlighting the essential mechanisms of optical processes. However, no minimal atomistic exciton model currently exists for ML MoS$_2$, making numerical approaches to, e.g., nonlinear optical properties, difficult. Given the recent interest [4–8] in the nonlinear, and in particular second harmonic (SH), properties of FL MoS$_2$ the development of such models appears particularly pressing.

Several authors [4–6,28] have recently demonstrated how second-harmonic-generation microscopy can be used to extract important information regarding, e.g., the number of layers and crystallographic orientation of few-layered MoS$_2$ platelets. Furthermore, exfoliated MoS$_2$ was shown experimentally to display a remarkably large SH signal, with SH susceptibilities on the order of ∼100 nm/V reported by the authors of Ref. [4] while the authors of Refs. [5,6] reported only ∼0.1 nm/V (assuming a homogeneous susceptibility inside the monolayer of thickness ∼3 Å when relating to sheet SH susceptibilities). The regions covered with an odd number of 2H stacked layers were found to generate SH fields with efficiencies decreasing slightly with the number of layers, while regions with an even number of layers displayed almost vanishing SH signals as expected due to centrosymmetry [4–6]. However, few-layered MoS$_2$ grown by chemical vapor deposition (CVD) does not follow this trend [4], possibly due to the stacking order of CVD-grown films deviating from 2H. In Ref. [5], SH spectra of both ML and trilayer (TL) MoS$_2$ were presented, demonstrating an intense peak in the SH spectrum at pump photon energies near 1.45 eV, with a slight redshift for TLs compared to MLs. Moreover, very recently the excitation of valley-coherent excitons was demonstrated using two-photon processes, such as SH generation, in the closely related system of ML WSe$_2$ [29]. This effect could

[*]mlt@nano.aau.dk

also be of importance in the nonlinear optical properties of ML MoS$_2$, perhaps opening avenues for exploring the rich valley physics [30] of this material using SH spectroscopy. There exists little theoretical work with which to interpret the experimental findings mentioned above. To our knowledge, the quasiparticle/exciton results by Grüning and Attaccalite [8][1] remains the only theoretical paper on SH generation in MoS$_2$. There it was demonstrated how electron-hole attraction significantly increases the magnitude of the second-harmonic signal relative to the one-electron result of the same paper, although few changes to the overall spectral shape of the response function were reported (in contrast to ML hexagonal boronnitride). Several issues regarding the excitonic SH response in monolayer MoS$_2$ remain, however. In Ref. [8], spin-orbit coupling (SOC) was neglected, which in linear optics generates a very distinct splitting of the fundamental exciton peak on the 100-meV scale [2]. Hence, while the corresponding features in the SH spectrum might be expected to split in a similar manner, the more complicated resonance structure of the SH spectrum makes it difficult to predict the effects of SOC on the SH spectrum, without performing the full calculation, for anything but the case of SH energies near the absorption edge. Also, in their work, Grüning and Attaccalite applied a model avoiding the direct diagonalization of the Bethe-Salpeter equation implicit in other models of SH generation, such as the work by Leitsmann *et al.* [31], relying instead on a time-integration scheme. While this approach undoubtedly has many benefits, the Bethe-Salpeter approach remains the most universally applied method for the calculation of optical excitations in crystalline semiconductors and simplifies formally to the historically important single-particle results generated using, e.g., the formalism of Moss and Sipe [32,33] in the limit of infinite electron-hole screening [31]. However, at present, it is very computationally demanding to retain the k-space resolution needed to resolve delicate spectral features in a full exciton calculation — a problem which is even more pronounced in the calculation of nonlinear response functions since these tend to converge rather slowly. This is also evident in Ref. [8], where the relatively coarse k grid ($21 \times 21 \times 1$ points) imposes substantial broadening on the resulting spectrum, making it difficult to resolve, e.g., the bound exciton states below the band gap (i.e., the SH counterpart to the A and B features of linear optics) and the underlying structure of the observed broadened features.

In the present work, we consider the microscopic origins of the SH response of ML MoS$_2$, including both SOC and excitonic effects in the Bethe-Salpeter picture [31], with a k-point resolution an order of magnitude better than for any SH exciton calculation previously published [8,31]. This clearly elucidates the spectral resonance structure of the SH spectrum imposed by bound electron-hole pairs. To accomplish this, we apply a model based on several components new to both MoS$_2$ research and excitonic SH response calculations in general. First, we apply a semi-empirical approach based on a tight-binding sp^3d^5 band structure recently published [34],

and an Ohno-like electron-electron interaction potential to setup the Bethe-Salpeter equation (BSE). Second, we block-diagonalize the BSE in both spin and out-of-plane parity of the tight-binding basis allowing a major reduction in the complexity of the problem. Third, we present a novel approach to the evaluation of the SH response, based on the BSE and the formalism found in Ref. [31], using a Lanczos method to avoid direct diagonalization of the exciton matrix. We note that our method is not restricted to MoS$_2$, and can readily be generalized for *ab initio* methods. Applying this model, we verify that the experimental measurements in Refs. [5,6] agree to within an order of magnitude with our model, and proceed to analyze the resonance structure of the SH spectrum. We find clear evidence of the A, B, and C features known from linear optics [1,2,12] also as resonances in the SH spectrum. Hence, a rich resonance structure, depending strongly on electron-hole interaction, is found for the SH spectrum of MoS$_2$. These findings can only be confirmed experimentally by renewed efforts in the measurement of SH spectra in a larger frequency range than has been published so far [5].

The remainder of this text is organized as follows. In the following section, the theoretical model is considered. Here, the approach to the electronic structure is first reviewed explaining the simplifications introduced in the one-electron tight-binding model followed by extension to the exciton picture by including electron-hole attraction. Following this, the model for calculating the linear and SH response is presented with a focus on the Lanczos implementation of SH response calculations. Finally, the results are presented and a conclusion is given.

II. THEORY AND METHODS

A. Electron states

It is well known that the valence and conduction band extrema of ML MoS$_2$ are located at the K points of the Brillouin zone and are dominated by d orbitals localized on the Mo atoms [35]. These bands are particularly important for optical transitions in the visible range, and are well represented by the tight-binding band structure found in Ref. [34]. However, a significant SOC due to the heavy Mo atoms causes a $\sim$100 meV splitting of the two highest valence bands near the K and K' points. To properly account for this we include SOC between the d orbitals localized on the same Mo atom [36], instead of the p orbitals used in the original parametrization [34]. We fit the SOC parameter $\lambda_{d,\text{Mo}} = 64$ meV to the 112-meV splitting of the two highest valence bands at K reported in Ref. [1].

Furthermore, it is found that SOC matrix elements off-diagonal in the spin index influence the final band structure very little, and hence we neglect these making the tight-binding block diagonal in spin. Moreover, we note that ML MoS$_2$ is spatially symmetric with respect to the reflection operation ($z \rightarrow -z$), taking all Mo in the plane $z = 0$. This is reflected by the atomic Mo orbitals, where the orbitals symmetric in z $\{s, p_x, p_y, d_{z^2}, d_{xy}, d_{x^2-y^2}\}$ couple to the antisymmetric group $\{p_z, d_{xz}, d_{yz}\}$ only in the off-diagonal SOC part of the Hamiltonian. The same can be stated for symmetric and antisymmetric combinations of orbitals centered on the S
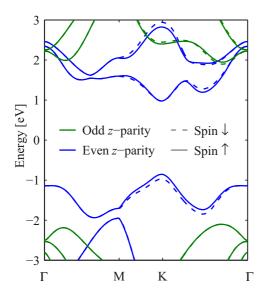

FIG. 1. (Color online) Band structure of ML MoS$_2$. Dashed/full lines indicate spin, whereas colors are used to indicate the parity of the bands with respect to the reflection through the MoS$_2$ sheet (see text for further discussion).

atoms, hence the mentioned neglect of off-diagonal SOC also allows for an electronic structure with bands of well-defined z parity. This is a tremendous computational advantage when considering the exciton problem, as will be discussed shortly.

The band gap of 1.8 eV generated using this method is comparable to the DFT band gap [1,34] of 1.7–1.8 eV and the experimentally recorded optical absorption edge [2,5,6,37] of 1.9 eV. However, it should be noted that the agreement between the DFT band gap and the experimental absorption peak arises from the approximate cancellation of the notorious DFT gap underestimation, corrected partially in the GW approximation, and the exciton binding energy [1,12,21]. Thus, we stress that even though similar results for, e.g., absorption edges can be obtained in the one-electron and exciton pictures, very different physics is, in fact, involved. Hence, to incorporate the correct quasiparticle gap necessary in an exciton calculation, we apply a simple scissor correction. The band structure of ML MoS$_2$ is displayed in Fig. 1 with no scissor shift. Only very little change relative to the original band structure [34] can be discerned even though our simplifications have allowed the separation of bands of even/odd z parity (blue/green lines) and up/down spin (full/dashed lines).

To include electron-hole attraction, exciton states are expanded in a basis of singly excited Slater determinants [24–26] $|(v\vec{k}) \to (c\vec{k})\rangle$, where a single valence band state v is excited to the conduction band c of the same k-vector. This approach is equivalent to a first-order configuration-interaction approach, and hence does not include multiply excited states such as the biexcitons [22] recently reported in MoS$_2$. Hence, the nth exciton wave function $|n\rangle$, with excitation energy E_n, is written as

$$|n\rangle = \sum_{c,v,\vec{k}} A^{(n)}_{cv\vec{k}} |(v\vec{k}) \to (c\vec{k})\rangle. \qquad (1)$$

Here $A^{(n)}_{cv\vec{k}}$ are expansion coefficients to be determined. We note that applying a basis of electron-hole configurations,

such as Eq. (1), is equivalent to applying the Tamm-Dancoff approximation (i.e., ignoring coupling between the resonant and antiresonant parts of the BSE) [38]. Including electron-hole attraction in an empirical tight-binding basis requires several approximations relative to the more sophisticated picture of full DFT + GW. Importantly, only tight-binding envelopes of the one-electron states are known, preventing direct evaluation of the Coulomb interaction matrix elements essential to an exciton calculation. Hence, these matrix elements are typically parametrized as simple functions of electron-hole separation distance (e.g., the Ohno-potential widely used for both organic [25] and inorganic [26] systems). We apply an effective Coulomb interaction on the Ohno form $V_C(\vec{r},\vec{r}') = -e^2/[4\pi\epsilon\epsilon_0\sqrt{|\vec{r} - \vec{r}'|^2 + a^2}]$, where a is an empirical parameter smearing the Coulomb singularity. Actually, this type of softened Coulomb interaction represents an effective way of including the layer thickness in quasi-two-dimensional systems [39–41], and a is hence taken to be on the order of the interlayer distance in MoS$_2$. A similar form also arises in models of two-dimensional gapped Dirac materials [42]. Furthermore, an effective screening parameter ϵ has been introduced. Using this two-particle interaction operator, the matrix problem yielding exciton energies E_n and expansion coefficients $A^{(n)}_{cv\vec{k}}$ is constructed in the basis of Eq. (1)

$$E_{cv\vec{k}} A^{(n)}_{cv\vec{k}} + \sum_{c',v'} \int W_{cv\vec{k},c'v'\vec{k}'} A^{(n)}_{c'v'\vec{k}'} \, d^2k' = E_n A^{(n)}_{cv\vec{k}}. \qquad (2)$$

Here, $E_{cv\vec{k}}$ represent quasiparticle energy differences between bands c and v at $\vec{k}$ in momentum space. In the derivation of the above expression, we have neglected the exchange term. Furthermore, Coulomb matrix elements

$$W_{cv\vec{k},c'\vec{v}'\vec{k}'} = \langle (v\vec{k}) \to (c\vec{k})|V_C|(v'\vec{k}') \to (c'\vec{k}')\rangle$$

$$= \iint \varphi^*_{c\vec{k}}(\vec{r})\varphi_{v\vec{k}}(\vec{r}')V_C(\vec{r},\vec{r}')\varphi_{c'\vec{k}'}(\vec{r})\varphi^*_{v'\vec{k}'}(\vec{r}')d^3r\,d^3r'$$

$$(3)$$

are evaluated by writing tight-binding states $\varphi_{\alpha\vec{k}}(\vec{r})$ as products of their rapidly varying lattice-periodic Bloch parts $u_{\alpha\vec{k}}(\vec{r})$ and slowly varying tight-binding envelopes $\exp(i\vec{k}\cdot\vec{r})$. The integral is then approximated by the unit-cell-averaged Bloch part products (contributing simply overlaps between Bloch functions) multiplied by the convolutions of the envelopes with the Coulomb interaction kernel over the entire domain of integration (contributing the Fourier transform of V_C) to yield

$$W_{cv\vec{k},c'v'\vec{k}'} \approx -\frac{e^2 I_{v'\vec{k}',v\vec{k}} I^*_{c'\vec{k}',c\vec{k}}}{8\pi^2\epsilon\epsilon_0|\vec{k} - \vec{k}'|} e^{-a|\vec{k}-\vec{k}'|}. \qquad (4)$$

The dominant contributions to the Bloch overlaps $I_{\alpha\vec{k},\beta\vec{q}}$ can be written in terms of elements from the k-dependent tight-binding overlap matrix $\overset{\leftrightarrow}{S}(\vec{k})$ and the tight-binding eigenvectors $\vec{C}_{\alpha\vec{k}}$

$$I_{\alpha\vec{k},\beta\vec{q}} = \frac{1}{\Omega_0} \int u^*_{\alpha\vec{k}}(\vec{r})u_{\beta\vec{q}}(\vec{r}) \, d^3r$$

$$\approx \frac{1}{2} \sum_{i,j} C^{(i)*}_{\alpha\vec{k}} C^{(j)}_{\beta\vec{q}} [S_{ij}(\vec{k}) + S_{ij}(\vec{q})]. \qquad (5)$$

Here, i and j are used to indicate the atomic basis, i.e., the entry of the one-electron eigenvector, and Ω_0 is the unit-cell area. With this, Eq. (2) is discretized on a uniform grid restricted to the Brillouin zone, and the matching two-particle exciton matrix $\overset{\leftrightarrow}{H}$ can be constructed. Exciton energies and states may then be obtained from direct diagonalization. However, this strategy becomes impractical even for modest k grids since $\overset{\leftrightarrow}{H}$ contains $N_{\text{exc}}^2 = (N_c \times N_v \times N_k)^2$ elements, N_c, N_v, and N_k indicating the number of conduction bands, valence bands, and k points, respectively. One simplification is to include only a restricted set of bands near the Fermi level in the one-electron basis. Additionally, since the quasiparticle states applied for the exciton calculation have a well-defined parity in z, the BSE may be diagonalized into blocks of even and odd symmetry. The same is true for spin, hence, only four diagonal blocks of the BSE contribute bright excitons, noting we consider the in-plane response. Moreover, in the optical response calculations to be discussed shortly we forego direct diagonalization completely and apply instead a Lanczos scheme [43].

B. Linear optical response

We calculate the real part of the diagonal, linear optical sheet conductivity tensor from the exciton states using the well-known expression [25]

$$\sigma'_{xx}(\omega) = \frac{e^2 \pi}{m_e^2 \hbar \omega \Omega} \sum_n |P_n|^2 \delta(\omega - \omega_n)$$
$$= \frac{e^2}{m_e^2 \omega \Omega} \text{Im}\langle P|G(w)|P\rangle, \quad (6)$$

where $\omega_n = E_n/\hbar$ and $P_n = \langle 0|\hat{P}_x|n\rangle$ indicate the transition frequency and the (in-plane) x component of the momentum matrix element coupling the nth exciton state with the ground state, while the crystal area is denoted Ω. Furthermore, $w = \omega + i\Gamma$ is the complex frequency containing the optical frequency ω and a small phenomenological broadening Γ, which should, strictly speaking, be taken to vanish for the second equality of Eq. (6) to hold. In practice, the sum over exciton states in the first line of Eq. (6) is rewritten in terms of matrix elements of the exciton Green's function $G(w) = \sum_n |n\rangle\langle n|/[\hbar w - E_n]$. Here, the state $|P\rangle = \hat{P}_x|0\rangle = \sum_{c,v,\vec{k}} p_{cv}^x |(v\vec{k}) \rightarrow (c\vec{k})\rangle$ is constructed from the x component of the all-electron momentum operator $\hat{P}$ acting on the ground state, while p_{cv}^x represents the x component of the one-electron momentum matrix elements between valence band v and conduction band c. This formulation has the advantage of allowing use of the Lanczos method for the evaluation of the resolvent matrix elements $\langle P|G(w)|P\rangle$ without having to directly diagonalize the BSE. In this approach, the Hamiltonian $\overset{\leftrightarrow}{H}$ is tridiagonalized into $\overset{\leftrightarrow}{T}$ by the similarity transformation $\overset{\leftrightarrow}{T} = \overset{\leftrightarrow}{Q}^\dagger \cdot \overset{\leftrightarrow}{H} \cdot \overset{\leftrightarrow}{Q}$. The transformation matrix $\overset{\leftrightarrow}{Q} = [\vec{q}_0\ \vec{q}_1, \ldots, \vec{q}_{N_{\text{exc}}-1}]$ can be constructed by recursive generation of the Lanczos vectors $\vec{q}_i$ and elements of $\overset{\leftrightarrow}{T}$ based on some initial seed vector $\vec{q}_0$. Additionally, since each recursion step only depends on the Lanczos vector of the previous step, this process may be halted at any point $j < N_{\text{exc}} - 1$. The resolvent matrix elements may

then be approximated in this restricted basis of typically a few hundred elements upon applying $|P\rangle$ as the initial Lanczos vector. A full review of this method may be found in Ref. [43].

In the one-electron limit (i.e., the limit $\epsilon \rightarrow \infty$), the exciton matrix Eq. (2) becomes diagonal, and the above expression reduces to purely one-electron contributions. In the limit of vanishing broadening, the real part of the response reduces to the one-electron result [44]

$$\sigma'_{xx}(\omega) = \frac{e^2}{2\pi m_e^2 \hbar \omega} \sum_{c,v} \int |p_{cv}^x|^2 \delta(\omega - \omega_{cv})\, d^2k, \quad (7)$$

where ω_{cv} denotes the transition frequency between states in bands c and v (with an implicit k dependence). One-electron momentum matrix elements are calculated as in Ref. [45]. In the one-electron limit, spectra fully converged with respect to k-point sampling can be generated using the improved linear-analytic triangle method [44]. This provides a basis for confirming the correct limiting behavior of the exciton spectrum for $\epsilon \rightarrow \infty$.

C. Second harmonic optical response

The imaginary part of the sheet SH susceptibility tensor, at fundamental pump frequency ω, can be calculated from a set of exciton states using an expression identical to the one derived by Leitsmann *et al.* [31]

$$\chi_{abc}^{(2)}(\omega) = -\frac{ie^3}{\epsilon_0 \hbar^2 m_e^3 \Omega} \sum_{m,n} \frac{1}{\omega_n \omega_{nm} \omega_m} \left\{ \frac{P_{0nm}}{[\omega_n - 2w][\omega_m - w]} \right.$$
$$\left. - \frac{P_{mn0}}{[\omega_n - w][\omega_m + w]} + \frac{P_{m0n}}{[\omega_n + w][\omega_m + 2w]} \right\}. \quad (8)$$

Here, $P_{ijk} = P_{ij}^a[P_{jk}^b P_{ki}^c + P_{jk}^c P_{ki}^b]/2$ where P_{ij}^a is the Cartesian a component of the momentum matrix element between exciton states i and j (while 0 indicates the ground state). Furthermore, $\omega_{nm} = \omega_n - \omega_m$. Due to symmetry, the only nonvanishing SH tensor elements are $\chi_{xxx}^{(2)} = -\chi_{xyy}^{(2)} = -\chi_{yyx}^{(2)} = -\chi_{yxy}^{(2)} \equiv \chi^{(2)}$, with the x axis aligned along an armchair direction. Malard *et al.* [5] and Kumar *et al.* [4] defined this direction differently relative to the indices of the contributing tensor elements. However, we follow the conventions of the authors of Ref. [5] and confirm these to be correct by numerical testing (which is also clear from symmetry since the armchair direction spans a mirror plane together with the z axis). We again avoid direct diagonalization of the exciton problem by applying a Lanczos-based method as follows. First, we consider the first term of Eq. (8) (which is the dominant contribution to the SH spectrum) upon rewriting it slightly and denoting it $\chi_A^{(2)}$

$$\chi_A^{(2)}(\omega) = \frac{e^3}{\epsilon_0 \hbar^2 m_e^2 \Omega} \sum_{m,n} \langle P| \frac{|n\rangle\langle n|}{[\omega_n - 2w]\omega_n} \hat{X} \frac{|m\rangle\langle m|}{\omega_m[\omega_m - w]} |P\rangle$$
$$= \frac{e^3}{2\epsilon_0 m_e^2 \Omega \omega^2} \langle P|[G(2w) - G(0)]$$
$$\times \hat{X}[G(w) - G(0)]|P\rangle. \quad (9)$$

Here, $\langle m|\hat{X}|n\rangle = \langle m|\hat{P}_x|n\rangle/[i\omega_{mn}m_e]$ is the x component of the position operator. Second, we again apply a Lanczos tridiagonalization of the exciton matrix, which gives access to a set of orthonormal Lanczos states [43] spanning the eigenspace of the exciton Hamiltonian $|q_i\rangle, i = [0, \ldots, N_{exc} - 1]$, where $|q_0\rangle = |P\rangle$. Now, applying the approximate completeness of the Lanczos states, we write

$$\chi_A^{(2)}(\omega) = \frac{e^3}{2\epsilon_0 m_e^2 \Omega \omega^2} \sum_{n,m} [G_{0n}(2w) - G_{0n}(0)] X_{nm}$$
$$\times [G_{m0}(w) - G_{m0}(0)]. \quad (10)$$

Here, $G_{0n}(w) = \langle q_0|G(w)|q_n\rangle$ is the off-diagonal resolvent matrix element in the Lanczos basis while $X_{nm} = \langle q_n|\hat{X}|q_m\rangle$ is the x component of the position matrix element, also in the Lanczos basis. By calculating the resolvent matrix elements in a truncated basis using an efficient tridiagonalization routine, the SH response may be calculated much more efficiently than in the case of direct diagonalization. Including all three terms of Eq. (8) yields upon rewriting to Green's functions in a similar manner

$$\chi^{(2)}(\omega) = \frac{e^3}{2\epsilon_0 m_e^2 \Omega \omega^2} \sum_{n,m} \{F_{0n}(2w) X_{nm} F_{m0}(w)$$
$$+ 2[F_{0n}(-w) X_{nm} F_{m0}(w)$$
$$- F_{0n}(-w) X_{nm} F_{m0}(-w)]\}, \quad (11)$$

where $F_{nm}(w) = G_{nm}(w) - G_{nm}(0)$.

In the one-electron limit and a complete basis, the purely interband part of the SH response reduces to [31–33]

$$\chi_{abc}^{(2)''}(\omega) = \frac{e^3}{2\pi m_e^3 \hbar^2 \epsilon_0 \omega^3} \sum_{c,v,l} \int \left[\frac{P_{vcl}}{\omega - \omega_{lv}} \delta(2\omega - \omega_{cv}) \right.$$
$$\left. + \left(\frac{P_{vlc}}{\omega + \omega_{cl}} + \frac{P_{clv}}{\omega + \omega_{lv}} \right) \delta(\omega - \omega_{cv}) \right] d^2k. \quad (12)$$

Here, $P_{ijl} = \text{Im}\{p_{ij}^a(p_{jl}^b p_{li}^c + p_{jl}^c p_{li}^b)\}/2$ and the band index l runs over all bands with the restriction $l \neq (c,v)$. The first term of the one-electron SH susceptibility Eq. (12) contributes when an electronic excitation frequency ω_{cv} resonant with the SH photon frequency 2ω can be found. This term is referred to as the 2ω term, and whenever the aforementioned criterion is satisfied while $\omega \approx \omega_{lv}$ a particularly powerful, so-called double resonance is found. Similar comments can be made regarding the ω terms that contribute whenever the condition $\omega = \omega_{cv}$ is fulfilled. The first term in the expression for the excitonic response Eq. (8) [i.e., the term retained in Eq. (9)] displays a similar resonance, only here the denominator vanishes whenever an excitation frequency can be found matching the fundamental or SH frequency. A double resonance is found when both of these criteria can be fulfilled simultaneously. In fact, the resonance structure can be brought out clearly by expanding in partial fractions similarly to Ref. [32]. Then, in the limit of vanishing broadening, the imaginary part becomes proportional to two terms containing, respectively, δ functions with vanishing arguments for fundamental and SH

frequencies matching exciton transition frequencies. The k integrations necessary for evaluation of the one-electron result are performed using the improved linear-analytic triangle method [44], where care is taken to analyze double resonances of Eq. (12) by subsequent refinement of the integration mesh. Having calculated the imaginary part of $\chi^{(2)}$, the real part is found by Kramers-Kronig transformation. Also, in the exciton calculation, a 67×67 k grid was applied and $N_v = N_c = 8$.

III. RESULTS AND DISCUSSION

The computational simplicity gained by introducing the empirical model described above for electron-hole interaction comes with the price of three additional empirical parameters, namely the effective screening ϵ, the smearing of the Coulomb interaction a, and the scissor shift Δ. We estimate these parameters by comparing the resulting real part of the optical conductivity calculated here with the experimental absorption spectrum of Ref. [6] and the fully *ab initio* calculation of Ref. [12]. In Fig. 2(a), we display the optical conductivity as a function of screening ϵ and photon energy $\hbar\omega$ relative to the excitation energy of the fundamental absorption peak E_A (denoted the A peak) for a few values of the smearing factor a. The experimental spectrum from Ref. [6] is displayed in a similar color scheme as the bars on the right. The scissor correction, determined for each ϵ and a, is found simply as the energy shift taking the A peak to the experimentally reported position [6] of $E_A = 1.88$ eV. This value of Δ is plotted as the dashed curve. Several clear trends are observed: Two absorption peaks (termed the A and B peaks) dominate the fundamental absorption edge. These features represent bound exciton states, which in the basis of Eq. (1) can be mapped onto single-particle excitations near the K and K' points from the two highest parabolic SOC split valence bands to the lowest spin-degenerate conduction bands. Features similar to the A and B peaks can be found at excitation energies ~0.5 eV larger than the A excitation, moving closer to the A and B peaks with increasing screening. These are comparable to the A$'$ and B$'$ features recently reported in Ref. [12]. In that work, it was also demonstrated how the inclusion of electron-phonon interaction effectively smeared out the A$'$ and B$'$ peaks, explaining their absence from the experimental spectrum [6]. The spectral range between 0.5 and 1 eV relative to the A peak is dominated by a resonant state, in good agreement with previous theoretical findings, and is typically identified as the C peak [1,12]. This feature appears to be red-shifted relative to the corresponding experimental peak, however, Qiu *et al.* [12] demonstrate how electron-phonon interaction tends to merge and blue-shift the A$'$, B$'$, and C features, forming a broad peak near 2.9 eV reproducing the experimental spectrum closely.

We choose the values $\epsilon = 2.63$, $a = 6$ Å, $\Delta = 500$ meV, and display the corresponding linear spectrum in Fig. 2(b).

The applied screening parameter is on the order of dielectric functions reported by others [1,20,46], whereas the applied smearing a is approximately equal to the interlayer distance [21,34,47] in MoS$_2$.

Good agreement with experiment, on par with earlier *ab initio* results, is found [1,12] (noting that electron-phonon interaction is expected to, as mentioned, smear out the A$'$ and B$'$ features and "blue-shift" the C peak as in Ref. [12]) although
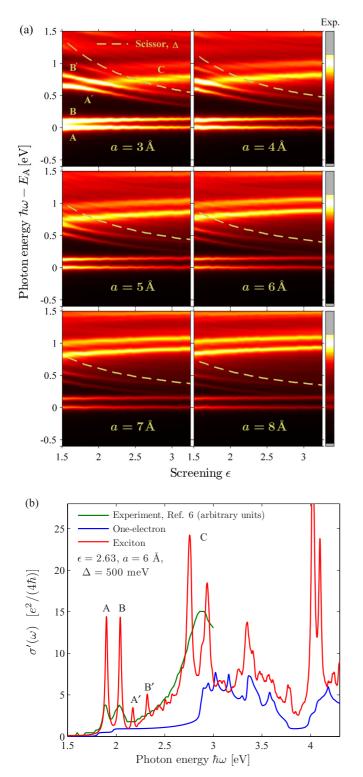
FIG. 2. (Color online) (a) Linear optical sheet conductivity for varying exciton screening parameters ϵ and smearing factors a as a function of photon energy relative to E_A. (b) Linear optical sheet conductivity of a MoS$_2$ ML calculated using the chosen parameters compared with the single-particle and experimental results from Ref. [6] (the latter in arbitrary units). A phenomenological broadening of $\hbar\Gamma = 10$ meV has been applied.

our model tends to overestimate the oscillator strengths of the A and B peaks relative to the C feature when compared to

experiments and other theory. We note that errors in, e.g., peak positions due to the neglect of exchange interaction may be compensated by fitting of the empirical parameters. Furthermore, the overestimation in A/B peak intensity and the slightly smaller scissor correction than was predicted *ab initio* in Ref. [12] may be partly due to neglect of exchange interaction.

The calculated SH susceptibility of a MoS$_2$ ML is shown in Fig. 3(a), both at the one-electron (top) and exciton (bottom) level. A small phenomenological broadening of 10 meV has been applied.

In the one-electron picture, the dispersion of the low-energy response near half the band gap is due to the 2ω term of Eq. (12) only, and can, in analogy with the linear case, be interpreted as optical transitions, for which the SH photon energy matches transitions from the highest valence band to the lowest conduction band near the K and K' points.

Two peaks are observed at fundamental photon energies corresponding to half the photon energies of the A and B peaks in the linear spectrum, although these are much weaker relative to the remaining spectrum when compared to the corresponding step heights in Fig. 2(b). Hence, we have included a magnified view of this spectral region on the left in Fig. 3(a). These peaks correspond to 2ω processes, and are here termed the A/2 and B/2 features since they appear at half the pump photon frequency of the corresponding linear peaks.

In this spectral region, the main difference upon including scissor shift and excitonic effects is the fact that a superposition of excited states, constructed from one-electron excitations near the K and K' points, now yields only a single excited state at the A/2 and B/2 positions (as opposed to step functions in the density of excited states, as was the case for the one-electron response). Hence, in the exciton picture, the A/2 and B/2 peaks are much narrower and more symmetric than in the one-electron case, but due to the near cancellation of quasiparticle and exciton energy shifts, they are found at approximately the same spectral position as the one-electron features. Furthermore, a shift in oscillator strength enhancing the B/2 peak slightly is observed.

Similarly, one might expect peaks corresponding to ω processes at twice the fundamental photon energy. However, in this region, 2ω processes close to double resonance dominate, making the ω features difficult to observe.

Also, an intense peak is found in both the one-electron and excitonic SH spectrum at fundamental photon energies ~1.45 eV corresponding to half the energy of the C transition. We denote this feature C/2, and note that its spectral position fits very well with the experimentally observed SH generation peak at 1.45 eV of Ref. [5]. This can readily be seen in Fig. 3(b), where we compare our theoretical calculations (now including a broadening of 30 meV realistic for comparison with room-temperature experiments) with the spectrum recorded by Malard *et al.* [5]. Again, we stress that the good agreement of the one-electron result with the experimental spectrum is rather deceptive since single-particle results generated using a corrected band gap by including quasiparticle effects at the scissor shift level in Eq. (12) completely fail to reproduce the experimental peak position.

Even though a good agreement with experiments in peak position and shape is generally observed for the one-electron and exciton spectra, a rather large intensity difference is also
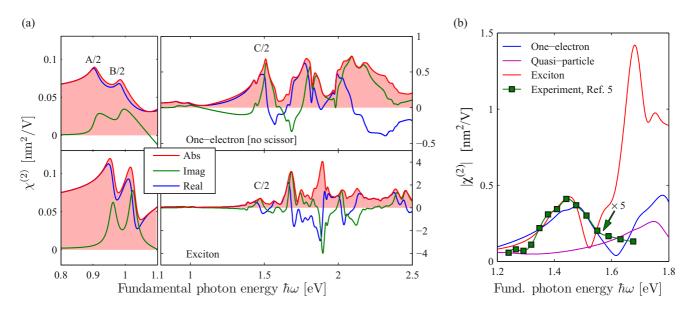
FIG. 3. (Color online) (a) Second harmonic sheet response of MoS$_2$ ML. (b) Comparison between experimental and theoretical SH susceptibilities. A phenomenological broadening of $\hbar\Gamma = 10$ meV has been applied in panel (a), while in (b) $\hbar\Gamma = 30$ meV.

found, with calculated results roughly five times larger than the experimental findings [5]. We note that this discrepancy with the experiment is smaller than the value previously reported [8], however. We attribute this to the fact that the denser k-point sampling in our work allows resolution of the weak peak at 1.4 eV (a much more intense, slightly blue-shifted peak would follow from merging of the 1.4 eV feature with the 1.65 eV peak if broadening of $\hbar\Gamma \sim 100$ meV was applied).

Additionally, we stress that Kumar *et al.* [4] reported susceptibilities two orders of magnitude larger than those calculated by us (although it should be noted that these results are not recorded relative to a known SH reference, as in Ref. [5], introducing a large degree of uncertainty). Hence, some uncertainties in the experimentally determined susceptibilities must be expected for an atomically thin material.

Also, we here compare theoretical results calculated for a free-standing MoS$_2$ sheet with experiments performed on a substrate where, e.g., strain or substrate phonons may be important.

Thus, while we expect some disagreement between the theory and experiment in the observed peak intensity, we believe its position and shape are reproduced rather well. Additionally, we expect the order of magnitude of the off-resonance susceptibilities reported here to be realistic.

On a final note, we stress that only one experimental SH spectrum in a rather narrow energy range has been published for ML MoS$_2$ to date [5]. Hence, a full comparison of the theoretical and experimental SH resonance structure cannot be made yet. In particular, it is of fundamental interest to resolve the A/2 and B/2 peaks experimentally.

A comparison between the exciton and one-electron spectrum leads us to several conclusions regarding the effects of excitons on the SH signal. First, in systems where the scissor correction and exciton binding energy approximately cancel, the low-energy features of the one-electron and exciton spectra agree qualitatively, although it should be noted that features arising from bound excitons become narrower and more sym-

metric compared to the one-electron result. Second, oscillator strength does not appear to transfer automatically to low-energy features to the degree observed in linear optics upon including electron-hole attraction. However, relative intensity redistribution (as compared to the one-electron calculation) may occur, although general trends are difficult to predict. Third, in systems with a large exciton binding energy, the resonance structure of the SH spectrum changes dramatically, removing and adding resonances. This is particularly clear for the powerful peaks near 1.65 and 1.9 eV in the exciton SH spectrum not found in the one-electron case.

IV. CONCLUSION

In conclusion, we have presented a new theoretical method for evaluating SH response functions expanding upon the work of Leitsmann *et al.* [31], which can quite generally be implemented in any Bethe-Salpeter framework. We have applied this method to MoS$_2$, and demonstrate that the inclusion of excitons has a dramatic impact on the SH spectrum of this material. We find clear signatures of the A, B, and C excitations, known from linear optics, also in the SH spectrum at fundamental photon energies near half the corresponding resonance energies in linear optics. Upon including excitons, the A and B features become more symmetric and a slight shift in intensity towards the B peak is observed. In the spectral region between 1.2 and 1.7 eV we find good agreement of both the one-electron (neglecting quasiparticle effects) and exciton results with the experimental spectrum of Malard *et al.* [5]. We find the absolute values of the SH susceptibility reported in Refs. [6] and [5] to agree better with our results than those reported in Ref. [4]. For fundamental photon energies larger than 1.5 eV, excitonic effects are seen to dramatically alter the resonance structure of the SH response relative to the one-electron case, introducing particularly intense peaks near 1.65 and 1.9 eV, and generally enhancing the intensity.

[1] A. Molina-Sánchez, D. Sangalli, K. Hummer, A. Marini, and L. Wirtz, Phys. Rev. B **88**, 045412 (2013).

[2] K. F. Mak, C. Lee, J. Hone, J. Shan, and T. F. Heinz, Phys. Rev. Lett. **105**, 136805 (2010).

[3] A. Splendiani, L. Sun, Y. Zhang, T. Li, J. Kim, C.-Y. Chim, G. Galli, and F. Wang, Nano Lett. **10**, 1271 (2010).

[4] N. Kumar, S. Najmaei, Q. Cui, F. Ceballos, P. M. Ajayan, J. Lou, and H. Zhao, Phys. Rev. B **87**, 161403 (2013).

[5] L. M. Malard, T. V. Alencar, A. P. M. Barboza, K. F. Mak, and A. M. de Paula, Phys. Rev. B **87**, 201401 (2013).

[6] Y. Li, Y. Rao, K. F. Mak, Y. You, S. Wang, C. R. Dean, and T. F. Heinz, Nano Lett. **13**, 3329 (2013).

[7] G. A. Wagoner, P. D. Persans, E. A. V. Wagenen, and G. M. Korenowski, J. Opt. Soc. Am. B **15**, 1017 (1998).

[8] M. Grüning and C. Attaccalite, Phys. Rev. B **89**, 081102 (2014).

[9] G. Eda, H. Yamaguchi, D. Voiry, T. Fujita, M. Chen, and M. Chhowalla, Nano Lett. **11**, 5111 (2011).

[10] Z. Yin, H. Li, H. Li, L. Jiang, Y. Shi, Y. Sun, G. Lu, Q. Zhang, X. Chen, and H. Zhang, ACS Nano **6**, 74 (2012).

[11] R. S. Sundaram, M. Engel, A. Lombardo, R. Krupke, A. C. Ferrari, Ph. Avouris, and M. Steiner, Nano Lett. **13**, 1416 (2013).

[12] D. Y. Qiu, F. H. da Jornada, and S. G. Louie, Phys. Rev. Lett. **111**, 216805 (2013).

[13] J.-T. Liu, T.-B. Wang, X.-J. Li, and N.-H. Liu, J. Appl. Phys. **115**, 193511 (2014).

[14] K. S. Novoselov, D. Jiang, F. Schedin, T. J. Booth, V. V. Khotkevich, S. V. Morozov, and A. K. Geim, Proc. Natl. Acad. Sci. USA **102**, 10451 (2005).

[15] B. Radisavljevic, A. Radenovic, J. Brivio, V. Giacometti, and A. Kis, Nat. Nanotechnol. **6**, 147 (2011).

[16] L. F. Mattheiss, Phys. Rev. B **8**, 3719 (1973).

[17] K. Kobayashi and J. Yamauchi, Phys. Rev. B **51**, 17085 (1995).

[18] T. Li and G. Galli, J. Phys. Chem. C **111**, 16192 (2007).

[19] A. Kuc, N. Zibouche, and T. Heine, Phys. Rev. B **83**, 245213 (2011).

[20] T. Cheiwchanchamnangij and W. R. L. Lambrecht, Phys. Rev. B **85**, 205302 (2012).

[21] H.-P. Komsa and A. V. Krasheninnikov, Phys. Rev. B **86**, 241201 (2012).

[22] E. J. Sie, Y.-H. Lee, A. J. Frenzel, J. Kong, and N. Gedik, arXiv:1312.2918.

[23] T. G. Pedersen and H. D. Cornean, Europhys. Lett. **78**, 27005 (2007).

[24] V. Perebeinos, J. Tersoff, and P. Avouris, Phys. Rev. Lett. **92**, 257402 (2004).

[25] T. G. Pedersen, Phys. Rev. B **69**, 075207 (2004).

[26] K. Leung and K. B. Whaley, Phys. Rev. B **56**, 7455 (1997).

[27] S. V. Goupalov, Phys. Rev. B **84**, 125407 (2011).

[28] X. Yin, Z. Ye, D. A. Chenet, Y. Ye, K. O'Brien, J. C. Hone, and X. Zhang, Science **344**, 488 (2014).

[29] G. Wang, X. Marie, I. Gerber, T. Amand, D. Lagarde, L. Bouet, M. Vidal, A. Balocchi, and B. Urbaszek, arXiv:1404.0056.

[30] T. Cao, G. Wang, W. Han, H. Ye, C. Zhu, J. Shi, Q. Niu, P. Tan, E. Wang, B. Liu, and J. Feng, Nat. Commun. **3**, 887 (2012).

[31] R. Leitsmann, W. G. Schmidt, P. H. Hahn, and F. Bechstedt, Phys. Rev. B **71**, 195209 (2005).

[32] E. Ghahramani, D. J. Moss, and J. E. Sipe, Phys. Rev. B **43**, 8990 (1991).

[33] T. G. Pedersen and K. Pedersen, Phys. Rev. B **79**, 035422 (2009).

[34] F. Zahid, L. Liu, Y. Zhu, J. Wang, and H. Guo, AIP Advances **3**, 052111 (2013).

[35] E. Cappelluti, R. Roldán, J. A. Silva-Guillén, P. Ordejón, and F. Guinea, Phys. Rev. B **88**, 075409 (2013).

[36] M. D. Jones and R. C. Albers, Phys. Rev. B **79**, 045107 (2009).

[37] R. F. Frindt, Phys. Rev. **140**, A536 (1965).

[38] M. Rohlfing and S. G. Louie, Phys. Rev. B **62**, 4927 (2000).

[39] S. Huang, Y. Liang, and L. Yang, Phys. Rev. B **88**, 075441 (2013).

[40] Y. E. Lozovik, I. V. Ovchinnikov, S. Y. Volkov, L. V. Butov, and D. S. Chemla, Phys. Rev. B **65**, 235304 (2002).

[41] C. Schindler and R. Zimmermann, Phys. Rev. B **78**, 045313 (2008).

[42] R. Petersen and T. G. Pedersen, Phys. Rev. B **80**, 113404 (2009).

[43] M. Grüning, A. Marini, and X. Gonze, Comp. Mater. Sci. **50**, 2148 (2011).

[44] T. G. Pedersen, C. Flindt, J. Pedersen, A.-P. Jauho, N. A. Mortensen, and K. Pedersen, Phys. Rev. B **77**, 245431 (2008).

[45] T. G. Pedersen, K. Pedersen, and T. B. Kriestensen, Phys. Rev. B **63**, 201101 (2001).

[46] A. H. Reshak and S. Auluck, Phys. Rev. B **68**, 125101 (2003).

[47] T. Böker, R. Severin, A. Müller, C. Janowitz, R. Manzke, D. Voß, P. Krüger, A. Mazur, and J. Pollmann, Phys. Rev. B **64**, 235305 (2001).